Applied Catalysis B: Environmental 148–149 (2014) 170–176

Contents lists available at ScienceDirect

Applied Catalysis B: Environmental

journal homepage: www.elsevier.com/locate/apcatb

Core–shell-structured carbon nanofiber-titanate nanotubes with enhanced photocatalytic activity

Soonhyun Kim*, Minsun Kim, Young Kwang Kim, Sung-Ho Hwang, Sang Kyoo Lim

Nano & Bio Research Division, Daegu Gyeongbuk Institute of Science and Technology (DGIST), Daegu 711-873, Republic of Korea

ARTICLE INFO

Article history:
Received 22 August 2013
Received in revised form 24 October 2013
Accepted 27 October 2013
Available online 2 November 2013

Keywords:
Core–shell
Carbon nanofiber
Titanate nanotubes
Photocatalytic activity

ABSTRACT

Core–shell materials have been developed extensively because of their advanced properties and multifunctionality. Many approaches involving different synthesis techniques have been used for the preparation of various core–shell nanostructures. In this study, we synthesized core–shell-structured carbon nanofiber (CNF)-titanate nanotubes (TiNT) by electrospinning, carbonization, and subsequent alkaline hydrothermal treatment. The CNF core could act as a support, and the TiO_2-decorated TiNT shell could act as a photocatalyst. TiNT shells with diameters of several hundreds of nanometers and composed of 10-nm-diameter nanotubes are formed on the CNF surface. The formation of TiNTs on the CNF surface was observed using SEM, HR-TEM, XRD, and XPS analyses. Core–shell-structured CNF-TiNTs exhibited efficient photocatalytic activities for CH_3CHO oxidation, which was attributed to the existence of photocatalytically active TiO_2-TiNT composites on the CNF surface, which could easily absorb UV light. Additionally, the surface area increase as a result of the alkaline hydrothermal treatment may also be responsible for the efficient photocatalytic activity of core–shell-structured CNF-TiNTs.

1. Introduction

TiO_2 photocatalysts have been intensively studied for application to the remediation of polluted water and air [1–3]. The photocatalytic reactions are initiated by the absorption of UV photons. The valence band (VB) electrons are excited into the conduction band (CB), simultaneously generating holes in the VB. Subsequently, the photogenerated electrons and holes initiate reduction and oxidation reactions at the surface, respectively. The electrons are consumed by electron acceptors, such as oxygen, and the holes react with electron donors, such as H_2O or hydroxyl groups, and produce hydroxyl radicals. However, some limitations of TiO_2 make it less efficient and hinder its more widespread application. One drawback is electron–hole recombination. The charge recombination and interfacial charge transfer rates depend on the surface properties of TiO_2. Therefore, to improve the photocatalytic activities of TiO_2 photocatalysts, many groups have tried to modify the TiO_2 surface by such approaches as noble metal deposition, inorganic anion adsorption, and surface charge modification [4].

For the practical application of TiO_2 photocatalysts, a number of studies have attempted to immobilize TiO_2 on different substrate materials, such as glass, zeolites, polymer fibers, and carbon materials [5–11]. Among these materials, carbon materials, such as activated carbon [12,13], carbon nanotubes [14–16], and carbon nanofibers (CNF) [17–19], have been frequently used as a support material. Recently, Ouzzine et al. investigated the photocatalytic activities of TiO_2 deposited on CNFs using a sol–gel method based on the properties of the CNFs and reported that it was difficult to deposit a homogeneous TiO_2 layer on CNFs [19]. Previously, we reported that TiO_2-particle-embedded CNFs prepared by electrospinning exhibited efficient photocatalytic activities [17]. Although the photocatalytic activity for gaseous acetaldehyde oxidation was efficient, TiO_2 was not homogeneously embedded. On the other hand, TiO_2 nanoparticles homogeneously embedded on CNFs could be obtained using non-aggregated nanosized TiO_2 particles prepared by the sol–gel method instead of pre-aggregated commercial Hombikat TiO_2 nanoparticles [20]. However, the photocatalytic activities were limited because the photoactive TiO_2 nanoparticles were entirely embedded in the CNFs and could not directly absorb UV light. Therefore, we tried to cover the CNF surface with photocatalytically active nanostructured TiO_2 materials, which has not been achieved via deposition by coating.

Core–shell materials have attracted much attention because they are expected to have advanced properties. ZnO nanowires have been grown radially on the fiber surface using a hydrothermal approach, and this microfiber–nanowire hybrid structure was used for energy scavenging [21,22]. Guo et al. have recently investigated core–shell CNF-TiO_2 nanosheets [18]. The TiO_2 nanosheets were grown directly on the CNFs by hydrothermal treatment in a solution containing fluorine ions. Recently, we investigated the formation of TiO_2-decorated titanate nanotubes (TiNTs) from TiO_2 nanoparticles under alkaline hydrothermal conditions [23,24]. Tang et al.

* Corresponding author. Tel.: +82 53 785 3410; fax: +82 53 785 3439.
E-mail address: sh2358@dgist.ac.kr (S. Kim).

0926-3373/$ – see front matter © 2013 Elsevier B.V. All rights reserved.
http://dx.doi.org/10.1016/j.apcatb.2013.10.051

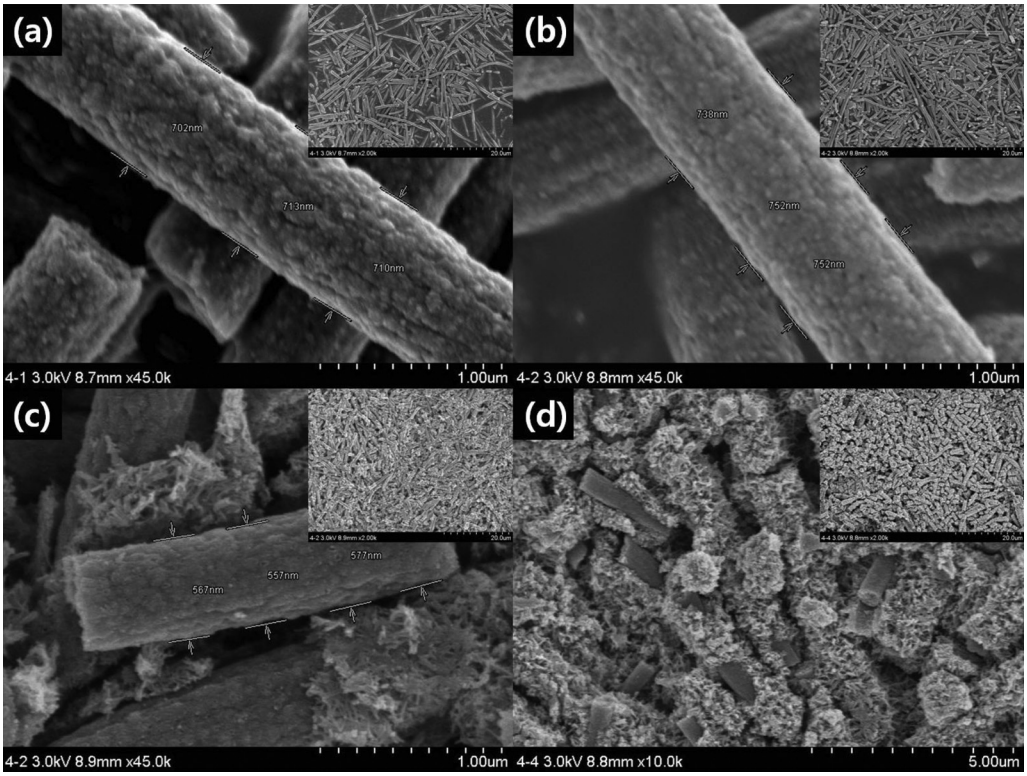

Fig. 1. FE-SEM images of (a) TiO_x/CNF, (b) TiO_2/CNF, (c) TiNT/CNF, and (d) TiO_2-TiNT/CNF.

also showed that TiNTs could be formed at the surface of the TiO_2 sphere template [25]. Based on these results, we expected TiNTs to form on the CNF surface by alkaline hydrothermal treatment.

In this study, we combined the electrospinning and hydrothermal methods to fabricate core–shell-structured CNF-TiNT composite nanostructures. First, a TiO_2-containing PAN solution was electrospun, and the obtained nanofiber webs were carbonized to produce CNFs with TiO_x nanoparticles. Second, the CNFs were hydrothermally treated with alkaline solution, after which TiNTs could form on the CNF surfaces. The obtained core–shell-structured CNF-TiNTs were characterized, and their photocatalytic activity for the oxidation of gaseous acetaldehyde was determined.

2. Experimental

2.1. Preparation of core–shell-structured carbon nanofiber-titanate nanotubes

TiO_x/CNFs were prepared by electrospinning/carbonization, as previously reported [17]. Nanosized TiO_2 synthesized by the sol–gel method was dispersed in 10 wt% polyacrylonitrile (PAN)/*N*,*N*-dimethylformamide (DMF) solution by stirring, and the mixture was sonicated to ensure good dispersal. The mass ratio of TiO_2 to PAN was 1:1. A yellow viscous TiO_2/PAN gel was electrospun, and the TiO_2/PAN nanofiber webs were collected. To obtain TiO_x/CNFs, the webs of TiO_2/PAN nanofibers were placed in a tube furnace, stabilized in air at 250 °C for 30 min, carbonized at 750 °C for 1 h, and then heated at 1400 °C in an N_2 atmosphere for an additional 1 h. The ramp rate was 5 °C/min between the 250, 750, and 1400 °C plateaus. TiO_2/CNFs could be obtained by the oxidation of TiO_x/CNFs by calcining at 400 °C for 3 h in air.

TiNT/CNFs were prepared by alkaline hydrothermal treatment, which is a typical method for synthesizing TiNTs from TiO_2 nanoparticles, as previously reported [23,24]. TiO_x/CNF were added to 200 ml of 10 M NaOH solution, hydrothermally reacted at 150 °C for 24 h, and then washed with 0.1 M HCl and distilled water. The obtained samples were denoted TiNT/CNF. The TiNT/CNFs were further calcined at 400 °C for 3 h in air. The calcined samples were denoted TiO_2-TiNT/CNF.

2.2. Characterization

The surface morphology images were obtained using a field emission scanning electron microscope (FE-SEM, Hitachi S-4200, Japan). Transmission electron micrographs were obtained on a high-resolution transmission electron microscope (HR-TEM, JEM-2200FS, Japan). The cross-sectional images of the samples were analyzed with a scanning transmission electron microscope (STEM, HD-2300, Hitachi, Japan). The samples were embedded in epoxy resin, cut into thin sections using an ultra-microtome, placed on Cu grids, and then analyzed. EDS X-ray diffraction (XRD) patterns were obtained with an X-ray diffractometer (Rigaku D/MAX-2500, 18 kV) using Cu-K_{a1} radiation. The oxidation states of C, Ti, O, N, and Na atoms were determined by X-ray photoelectron spectroscopy (XPS) (Kratos XSAM 800pci) using the Mg-K_α line (1253.6 eV) as the excitation source. The Brunauer–Emmett–Teller (BET) surface areas were determined from the nitrogen adsorption–desorption isotherms at 77 K (ASAP 2020 Micromeritics). The effective surface areas were estimated at a relative pressure (P/P_0) ranging from 0.01 to 0.1.

2.3. Photocatalytic activity measurements

The photocatalytic oxidation of gaseous CH_3CHO was determined in a closed circulated stainless steel reactor (volume, 150 cm^3) that could be divided into two parts (upper and bottom) by a control valve, similar to a previously reported experiment [17]. The gases used were CH_3CHO (300 ppmv N_2) as a CH_3CHO standard,

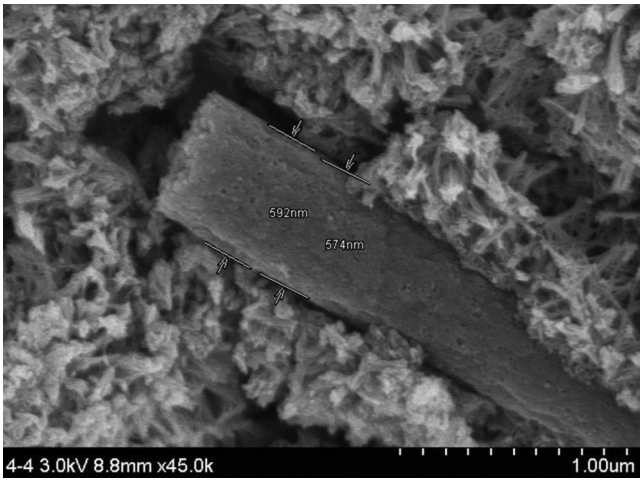

Fig. 2. High-magnification FE-SEM image of TiO_2-TiNT/CNF.

O_2 (99.9999%), and Ar (99.9999%) as the carrier gas. The concentrations of CH_3CHO and O_2 were 30–35 ppmv and 20%, respectively. A sample was placed onto the bottom reactor. All samples weighed approximately 15–25 mg and were in the form of 1.5 cm × 1.5 cm rectangular mats. First, the mixed gas passed through the empty upper reactor, and the concentration of CH_3CHO in the exit stream was monitored until it reached a constant value. The gas was then circulated in the reactor by the pump. Next, the circulated gas was passed through the bottom reactor by using the valve so that it came into contact with the surface of the sample placed in the bottom reactor. After adsorption equilibrium with the surface of the sample was established in the dark, the sample was illuminated with UV light (150-W Xe arc lamp, Abet Technologies). The distance between the sample and the lamp was 15 cm, and a cut-off filter ($\lambda < 295$ nm) was used. The removal of CH_3CHO was monitored using a gas chromatograph (GC, HP6890, Agilent) equipped with a Porapak Q column, a flame ionization detector (FID), a CO_2 methanizer (Ni catalyst), and a gas-sampling valve.

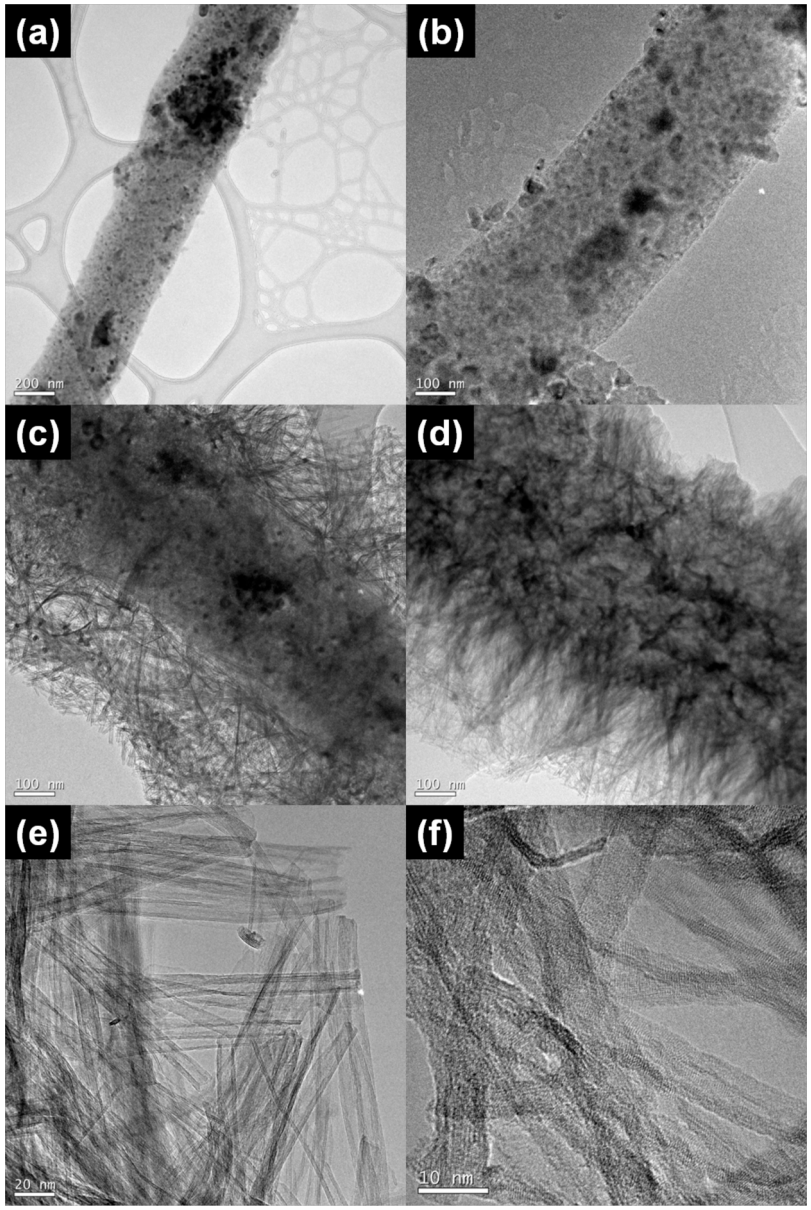

Fig. 3. HR-TEM images of (a) TiO_x/CNF, (b) TiO_2/CNF, (c) TiNT/CNF, (d) TiO_2-TiNT/CNF and high-magnification HR-TEM images of (e) TiNT/CNF and (f) TiO_2-TiNT/CNF.

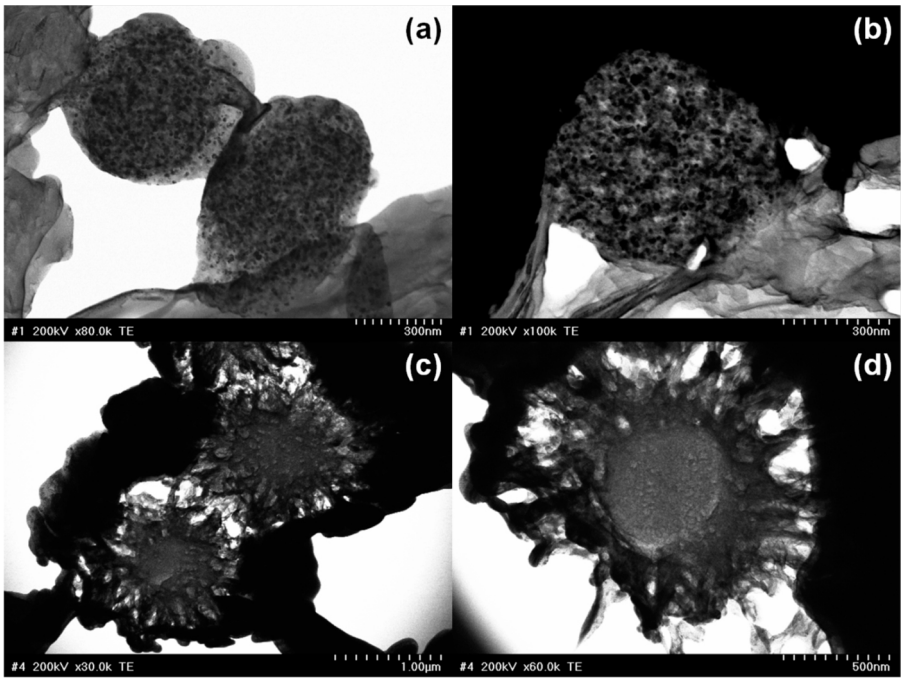

Fig. 4. Cross-sectional images of (a and b) TiO_x/CNF and (c and d) TiNT/CNF.

3. Results and discussion

3.1. Core–shell-structured carbon nanofiber-titanate nanotubes

The morphologies of the prepared samples were examined by SEM, as shown in Fig. 1. The diameter of the CNF core was 500–800 nm. In Fig. 1a, TiO_x particles are not clearly observed in the CNF, which might be due to the homogeneous dispersion, rather than aggregation, of the nanosized TiO_x particles. Fig. 1b shows that the morphology was not significantly changed by further heat treatment. However, after the hydrothermal treatment, the morphologies were significantly changed, and the TiNT shells were well formed on the CNF surface, as shown in Fig. 1c and d. The magnified image of the TiNT/CNFs in Fig. 1c shows that the bright TiNT seemed not to be well formed on the CNF surface compared to the magnified image of TiO_2-TiNT/CNF in Fig. 1d. This finding implies that the formation of TiNTs on the CNF surface was not uniform over the whole area. A high-magnification image of the TiO_2-TiNT/CNFs is shown in Fig. 2. It could be observed that the TiNTs aggregated and formed a shell on the CNF surface.

To study the microstructure, HR-TEM observations were carried out. Fig. 3a and b shows that the TiO_x or TiO_2 nanoparticles were not uniformly embedded in the CNF. The HR-TEM images of the TiNT/CNF in Fig. 3c and e shows that a shell comprised of smooth nanotubes was formed on the surface of the CNF core and that the diameter of the TiNTs was approximately 10 nm. After heat treatment, the TiNT nanotube structures remained, but the surfaces of the nanotube structures were rough. This roughness might be due to the potential recrystallization of the titanate structure induced by the heat treatment [26]. The formation of the TiNT shell was further confirmed by cross-sectional images and energy-dispersive spectroscopy (EDS), as shown in Fig. 4, Fig. S1, and Fig. S2. The EDS spectrum indicated that the dark spots in the CNFs and TiNTs on the CNF surface were composed of Ti. Therefore, the cross-sectional images clearly show that the alkaline hydrothermal treatment eliminated the Ti species in the CNFs and formed TiNTs on the CNF surface.

The XRD patterns are shown in Fig. 5. As observed in Fig. 5a, the diffraction peaks of TiO_x/CNF appeared at $2\theta = 36.9^\circ$, 42.8°, 61.9°, 74.2°, and 78.0°, corresponding to the reflection planes of (1 1 1), (2 0 0), (2 2 0), (3 1 1), and (2 2 2) of the cubic TiN structure, respectively [27]. This finding implied that the TiO_2 was reduced to TiN during carbonization under N_2 flow. The TiN peaks decreased in intensity for the other samples, indicating that the Ti species drastically changed during the calcination or alkaline hydrothermal treatment. In Fig. 5b, the XRD pattern of TiNT/CNF showed a weak peak corresponding to the (1 1 0) plane of TiNT, suggesting that TiNT could be formed on the CNF surface during the alkaline hydrothermal treatment. On the other hand, both TiO_2/CNF and TiO_2-TiNT/CNF exhibited a diffraction peak at $2\theta = 25.4^\circ$, which was attributed to the (1 0 1) crystal faces of the anatase TiO_2, indicating that TiN or TiNT was reoxidized to TiO_2 with an anatase structure during the calcination [17].

Fig. 6 compares the C 1s, Ti 2p, and O 1s XPS spectra of the prepared samples. The C 1s, Ti 2p, and O 1s peak intensities are clearly different before and after the alkaline hydrothermal reactions. Before the alkaline hydrothermal reactions, the C specie was dominant, whereas the Ti and O species were predominant over the surface of the samples after the alkaline hydrothermal reaction. This implies that the Ti species dissolved, moved to the CNF surface, transformed into titanate nanotubes, and then covered the entire surface of CNF during the alkaline hydrothermal treatment. The Ti $2p_{3/2}$ of TiO_x/CNF and TiO_2/CNF are located at the binding energies of 456.2 and 459.2 eV, respectively, which are consistent with the binding energies of TiN and TiO_2, respectively. This might be due to the reduction of TiO_2 to TiN during the carbonization process under N_2 flow and its re-oxidization to TiO_2 by calcination under air, as previously reported [17]. The O 1s peak of TiO_2/CNF was obviously shifted to a lower binding energy than that of TiO_x/CNF, which could be attributed to the incorporation of O species and the formation of Ti—O bonds. The existence of N and Na was also confirmed by XPS, as shown in Fig. 7. The N 1s peak was observed in the TiO_x/CNF and TiNT/CNF samples, which were obtained before the calcinations. This finding implies that the N species are oxidized to NO_x and are not present on the CNF surface after the calcination. The N 1s binding energy of 397.5 eV for the TiO_x/CNF sample is consistent with that of N^{3-}, which is attributed to the TiN [28]. The oxidation state of N 1s was changed by the alkaline hydrothermal reaction,

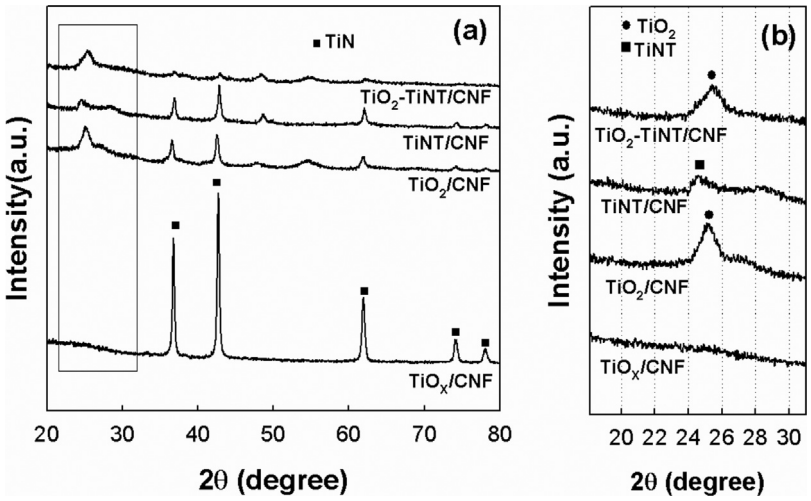

Fig. 5. XRD patterns of TiO_x/CNF, TiO_2/CNF, TiNT/CNF, and TiO_2-TiNT/CNF.

and the N 1s binding energy of 400–401 eV of the TiNT/CNFs could be attributed to the N species incorporated in the O—Ti—N bonding [28]. On the other hand, Na 1s was observed in the TiNT/CNF and TiO_2-TiNT/CNF samples because the Na was present as NaOH, which was added during the alkaline hydrothermal reaction. This result implies that the Na species are not completely removed during the washing process.

Based on the above results, the formation of TiNTs on the CNF surface could be explained as follows. First, the TiN embedded in the CNF was dissolved, moved to the CNF surface during hydrothermal treatment in NaOH solution, and then reacted with OH^- near the CNF surface. As a result, the TiN in the cores was consumed, and titanate nanosheets might be intermediately generated on the CNF surface. Subsequently, TiNT shells could be completely formed on the CNF surface. A schematic illustration of the formation of TiNT on the CNF surface is shown in Fig. 8. TiNT was formed according to the formation mechanism for the TiO_2-derived nanotubes via an alkaline hydrothermal process [29–33], which scrolls the titanate sheets. The formation of TiNT on the CNF surface could be easily observed. Images of TiO_x/CNF and TiNT/CNF are shown in Fig. S3. Before the alkaline hydrothermal treatment, the TiO_x/CNF was similar to the common CNF mat, whereas the TiO_2-TiNT/CNF surface was somewhat whitish due to the formation of TiNT, which is white.

3.2. Photocatalytic activities

The photocatalytic activity of the core–shell-structured CNF-TiNTs was evaluated by the photocatalytic oxidation of gaseous CH_3CHO. In Fig. 9, the photocatalytic CH_3CHO oxidation and simultaneous CO_2 production are shown. Before UV irradiation, the CH_3CHO gas was circulated and in contact with the samples. Therefore, the dark adsorption on the surface of samples under circulating condition could be monitored. The dark adsorption and the photocatalytic activities of TiO_x/CNF and TiO_2/CNF were negligible. On the other hand, TiNT/CNFs exhibited dark adsorption of CH_3CHO, whereas its photocatalytic activity was still negligible. The dark adsorption of TiNT/CNF and TiO_2-TiNT/CNF might be due to the high surface area, as shown in Table 1. The surface area was increased by the alkaline hydrothermal treatment as a result of the formation of TiNTs on the CNF surface, which could be responsible for the dark adsorption of CH_3CHO before irradiation. The TiO_2-TiNT/CNFs exhibited a much higher photocatalytic oxidation

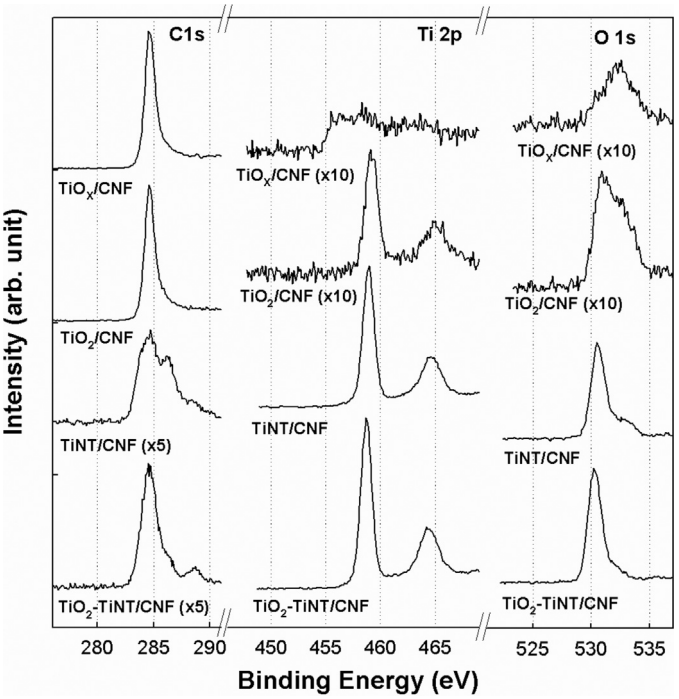

Fig. 6. C 1s, Ti 2p, and O 1s peaks in the XPS spectra of TiO_x/CNF, TiO_2/CNF, TiNT/CNF, and TiO_2-TiNT/CNF.

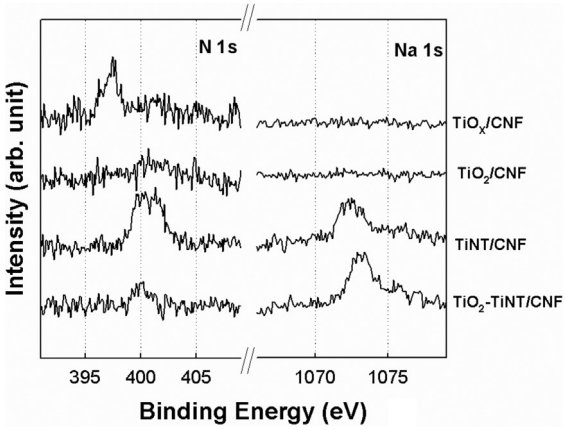

Fig. 7. N 1s and Na 1s peaks in the XPS spectra of TiO_x/CNF, TiO_2/CNF, TiNT/CNF, and TiO_2-TiNT/CNF.

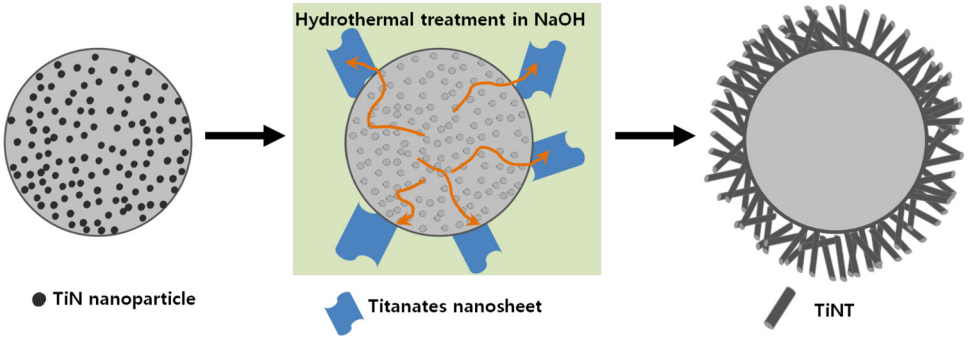

Fig. 8. A schematic illustration of the formation of TiNT on the CNF surface.

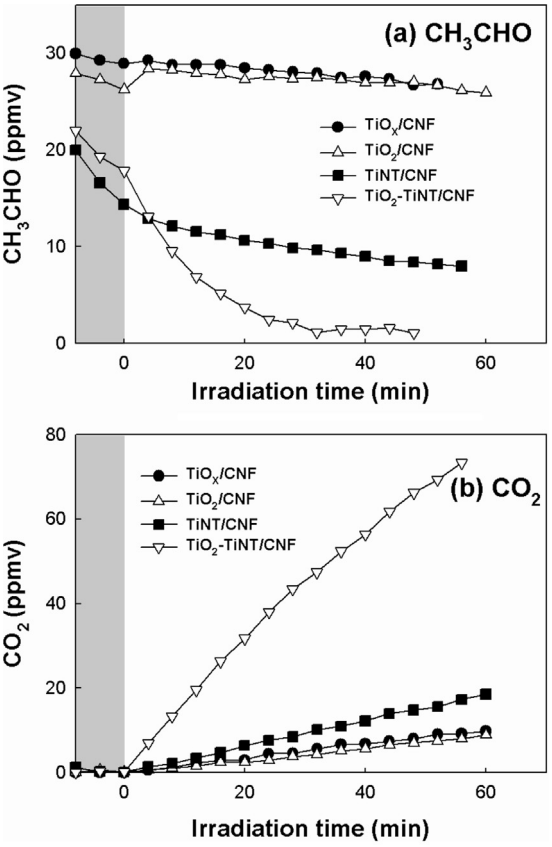

Fig. 9. (a) Photocatalytic degradation of gaseous CH_3CHO and (b) simultaneous production of CO_2 on TiO_x/CNF, TiO_2/CNF, TiNT/CNF, and TiO_2-TiNT/CNF.

efficiency. The photocatalytic activities of TiO_2-TiNT/CNF could be due to the anatase TiO_2. As previously reported, TiNTs have no photocatalytic activity, and further treatment, such as acid treatment or calcinations to partially produce anatase TiO_2 [23,34] are needed. On the other hand, although the TiO_2/CNF has an anatase crystalline structure due to further calcination, its photocatalytic activity was still negligible. It is possible that the photocatalytically active TiO_2 nanoparticles are homogeneously dispersed, and almost all TiO_2 nanoparticles are embedded in the CNFs. This implies that the TiO_2 nanoparticles in TiO_2-embedded CNF must be agglomerated to produce photocatalytic activity, as previously reported [17]. The core–shell-structured CNF-TiNTs with anatase TiO_2 nanoparticles had a higher surface area than the CNFs and exhibited efficient photocatalytic activity. Therefore, the alkaline hydrothermal treatment to form TiNTs on the CNF surface can be considered a suitable candidate for efficient photocatalyst composites of TiO_2-embedded CNF materials.

Table 1
BET surface areas of the prepared samples.

	BET surface area (m^2/g)
TiO_x/CNF	86.6
TiO_2/CNF	185.5
TiNT/CNF	302.3
TiO_2-TiNT/CNF	233.7

4. Conclusion

We synthesized core–shell-structured CNF-TiNTs by electrospinning/carbonization and subsequent alkaline hydrothermal treatment. First, TiO_2-embedded PAN nanofibers were prepared by electrospinning. Second, TiO_2-embedded PAN nanofibers were carbonized under N_2 flow, which reduced the TiO_2 nanoparticles and PAN nanofibers to TiN and CNFs, respectively, and TiN-embedded CNFs are formed. Finally, the TiN nanoparticles in CNF are dissolved, transferred to the solution, and then transformed into TiNTs on the CNF surface as a result of the alkaline hydrothermal treatment. The formation of TiNTs on the CNF surface was observed by SEM, HR-TEM, XRD, and XPS analysis. Core–shell-structured CNF-TiNT exhibited efficient photocatalytic activities for CH_3CHO oxidation. As previously reported, TiO_2-embedded CNFs could be a facile alternative environmental remediation materials for practical application and have potential applications in many fields, such as air or water purification, hydrogen production from water splitting, fuel cells, and hydrogen adsorption. This study suggests that the alkaline hydrothermal treatment of TiO_x- or TiO_2-embedded CNFs is a useful method to improve their adsorption and photocatalytic activities.

Acknowledgments

This work was supported by the DGIST R&D Program of the Ministry of Education, Science and Technology of Korea (13-NB-03).

Appendix A. Supplementary data

Supplementary material related to this article can be found, in the online version, at http://dx.doi.org/10.1016/j.apcatb.2013.10.051.

References

[1] M.R. Hoffmann, S.T. Martin, W.Y. Choi, D.W. Bahnemann, Chem. Rev. 95 (1995) 69–96.
[2] W. Choi, Catal. Surv. Asia 10 (2006) 16–28.
[3] S. Kim, W. Choi, Environ. Sci. Technol. 36 (2002) 2019–2025.

[4] H. Park, Y. Park, W. Kim, W. Choi, J. Photochem. Photobiol. C 15 (2013) 1–20.
[5] S. Matsuzawa, C. Maneerat, Y. Hayata, T. Hirakawa, N. Negishi, T. Sano, Appl. Catal. B: Environ. 83 (2008) 39–45.
[6] L. Ye, C.D.M. Filipe, M. Kavoosi, C.A. Haynes, R. Pelton, M.A. Brook, J. Mater. Chem. 19 (2009) 2189–2198.
[7] P. Lei, F. Wang, X.W. Gao, Y.F. Ding, S.M. Zhang, J.C. Zhao, S.R. Liu, M.S. Yang, J. Hazard. Mater. 227 (2012) 185–194.
[8] C. Su, Y. Tong, M. Zhang, Y. Zhang, C. Shao, RSC Adv. 3 (2013) 7503–7512.
[9] W. Li, Y. Bai, F. Li, C. Liu, K.Y. Chan, X. Feng, X. Lu, J. Mater. Chem. 22 (2012) 4025–4031.
[10] Y. Kuwahara, J. Aoyama, K. Miyakubo, T. Eguchi, T. Kamegawa, K. Mori, H. Yamashita, J. Catal. 285 (2012) 223–234.
[11] S. Anandan, M. Yoon, J. Photochem. Photobiol. C 4 (2003) 5–18.
[12] X. Zhang, M. Zhou, L. Lei, Carbon 43 (2005) 1700–1708.
[13] M.H. Baek, J.W. Yoon, J.S. Hong, J.K. Suh, Appl. Catal. A: Gen. 450 (2013) 222–229.
[14] Q. Huang, L. Gao, J. Mater. Chem. 13 (2003) 1517–1519.
[15] W.D. Wang, P. Serp, P. Kalck, C.G. Silva, J.L. Faria, Mater. Res. Bull. 43 (2008) 958–967.
[16] G.M. An, W.H. Ma, Z.Y. Sun, Z.M. Liu, B.X. Han, S.D. Miao, Z.J. Miao, K.L. Ding, Carbon 45 (2007) 1795–1801.
[17] S. Kim, S.K. Lim, Appl. Catal. B: Environ. 84 (2008) 16–20.
[18] W.X. Guo, F. Zhang, C.J. Lin, Z.L. Wang, Adv. Mater. 24 (2012) 4761–4764.
[19] M. Ouzzine, M.A. Lillo-Ródenas, A. Linares-Solano, Appl. Catal. B: Environ. 127 (2012) 291–299.
[20] S. Kim, S.K. Choi, S.K. Lim, D. Chang, H. Park, Cryst. Res. Technol. 45 (2010) 1079–1082.
[21] Y. Qin, X.D. Wang, Z.L. Wang, Nature 451 (2008), 809–U805.
[22] J.W.P. Hsu, Z.R. Tian, N.C. Simmons, C.M. Matzke, J.A. Voigt, J. Liu, Nano Lett. 5 (2005) 83–86.
[23] S. Kim, M. Kim, S.H. Hwang, S.K. Lim, J. Ind. Eng. Chem. 18 (2012) 1141–1148.
[24] S. Kim, M. Kim, S.H. Hwang, S.K. Lim, Appl. Catal. B: Environ. 123–124 (2012) 391–397.
[25] Y.F. Tang, L. Yang, J.Z. Chen, Z. Qiu, Langmuir 26 (2010) 10111–10114.
[26] C.H. Lin, J.H. Chao, C.H. Liu, J.C. Chang, F.C. Wang, Langmuir 24 (2008) 9907–9915.
[27] J.H. Bang, K.S. Suslick, Adv. Mater. 21 (2009) 3186.
[28] X. Chen, Y. Low, A.C.S. Samia, C. Burda, J.L. Gole, Adv. Funct. Mater. 15 (2005) 41–49.
[29] T. Kasuga, M. Hiramatsu, A. Hoson, T. Sekino, K. Niihara, Langmuir 14 (1998) 3160–3163.
[30] A. Nakahira, T. Kubo, C. Numako, Inorg. Chem. 49 (2010) 5845–5852.
[31] D.V. Bavykin, F.C. Walsh, Titanate and Titania Nanotubes: Synthesis, Properties and Applications, Royal Society of Chemistry, Cambridge, 2010.
[32] K. Kiatkittipong, C. Ye, J. Scott, R. Amal, Cryst. Growth Des. 10 (2010) 3618–3625.
[33] K. Kiatkittipong, J. Scott, R. Amal, ACS Appl. Mater. Inter. 3 (2011) 3988–3996.
[34] H.Y. Zhu, Y. Lan, X.P. Gao, S.P. Ringer, Z.F. Zheng, D.Y. Song, J.C. Zhao, J. Am. Chem. Soc. 127 (2005) 6730–6736.